Measurement of Tire Tread Depth with Image Triangulation

Shih-Yen Huang[1*], Yen - Cheng Chen[2], Jih-Kai Wang[3]

Department of Computer Science and Information Engineering

National Chin-Yi University of Technology, Taiwan

Taichung, Taiwan

[1]syhuang@ncut.edu.tw

[2]B99170105@gmail.com

[3]wangs51111@gmail.com

***Abstract*—Tires bear the grip and friction force between a vehicle and the ground. Worn tires will result in slippage, a longer braking distance, and even flat tires, which could eventually result in a driving accident. Therefore, governments, including Taiwan, have formulated standards stipulating the appropriate tire pressure and depth of tire treads.**

The tire tread depth used to be determined using manual contact measurement. This study created a non-contact measurement prototype system which applying machine vision to measure tread depth that uses image triangulation to reduce the manpower expense and improve the convenience of measurement.

Based on the Epipolar plane, this system obtains the distance between the tire treads and camera lens, consequently, the depth image of the tire tread was constructed. Along with the normal direction of groove of the tire's main tread on the depth images, obtaining the correct depth data using the majority decision voting strategy. Consequently, the tread depth was measured. In addition, this system produced an application (APP) which allows a user to obtain and record the tire tread depth on their Android smart phone.

***Keywords*— Machine vision, Epipolar plane, tread depth, non-contact measurement, smart phone**

I. INTRODUCTION

Image processing is widely used in various fields. It includes image segmentation, image classification, image recognition, edge detection, image compression, image noise filtering, and depth measurement [1], which obtains the depth of an object's baseline mainly by matching and triangulation.

Governments around the world have placed emphasis on testing tires in recent years, especially to determine the tire pressure and tread, to improve driving safety. A lack of tire treads will result in an inadequate grip force, which affects the driving safety of the vehicle. Therefore the American Federal Motor Carrier Safety Administration (FMCSA) stipulates that the depth of tire treads should be at least 2/32 of an inch [2].

The Ministry of Transportation and Communications of Taiwan lists the depth of tire treads as a periodic inspection item to guarantee driving safety. The depth of tire treads should be larger than 1.6 mm [3], with the wearing degree of the wearing indicator as the reference.

The tire tread depth used to be measured using manual contact measurement. This study created a non-contact measurement prototype system which applying machine vision to measure tread depth that uses image triangulation to reduce the manpower expense and improve the convenience of measurement.

This system measures the depth of tire treads using Labview stereo vision, and can determine the correct depth in the tread's region of interested (ROI) using image processing for edge detection. In addition, this allows a user to acquire information about the depth through the Internet or a phone by connecting to a database with the Internet of Things.

II. SYSTEM DESIGN

Two identical cameras were set in parallel on a camera base, and four light sources were placed on all four sides of the camera base, as shown in Fig. 1. Depth images could be obtained after the images from the two cameras were calculated using the stereo vision function of Labview. The tire tread depth could be calculated by analyzing the relative distance between the surface and groove of the tire treads inside the ROI. The tire tread depth was then uploaded to the phone or tablet of a user through a MySQL database. See Fig. 2 for the detailed process.

A. Camera Base

This study analyzed the distance between the cameras and the object using the Epipolar plane, which required that the cameras meet the following two conditions.

(1) The cameras have the same focal distance f.

(2) The cameras are placed on the same horizontal axis in parallel.

The camera base designed in this study is shown in Fig. 1. Light sources that could independently control the angles and brightness were placed on the four sides of the camera base to influence the image quality.

978-1-5090-3071-2/16 $31.00 © 2016 IEEE
DOI 10.1109/IS3C.2016.86

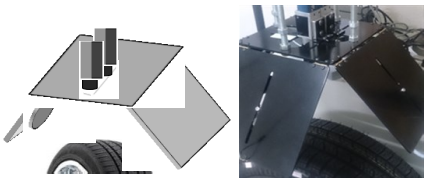

Fig. 1 Real stereo vision environment

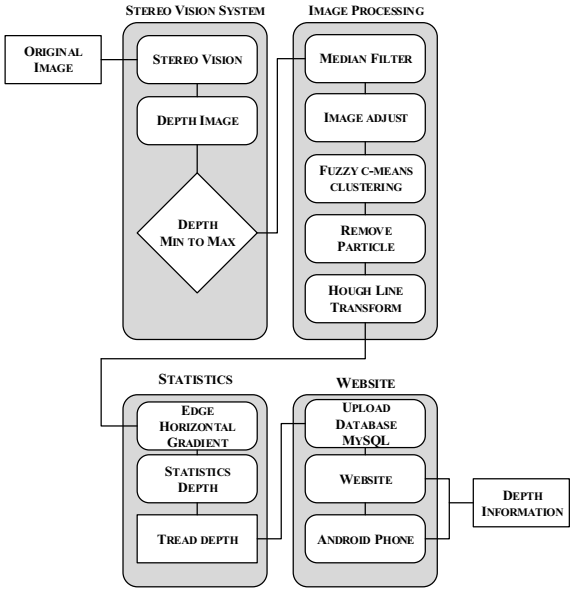

Fig. 2 System flow chart for inspecting tread depth automatically

B. Epipolar Plane

The center points of both cameras were set on the left and right of the horizontal axis using points B and C, according to the Epipolar plane (Fig. 3). Point A represents a point of the object, where (x, y, z) are the three-dimensional space coordinates in the real word with point B as the origin, z stands for the vertical distance between point A and the cameras, and b stands for the distance between the center points of the left and right cameras. The plane formed by points A, B, and C was called the Epipolar plane, where $\overline{BC}$ is the baseline [4].

The image of point A at the left camera is point G, and that on the right camera is point I. Formula (1) can be obtained according to the trigonometric proportional relation $\Delta BFG \approx \Delta BDA$; formula (2) can be obtained according to the trigonometric proportional relation $\Delta CHI \approx \Delta CEA$; and by regarding point B of the coordinate system as the origin, formula (3) can be obtained by utilizing the horizontal axis coordinate X_l of point G on the left camera's image and coordinate X_r of point I on the right camera's image in formula (1) and formula (2) to determine the vertical distance z of corresponding point A.

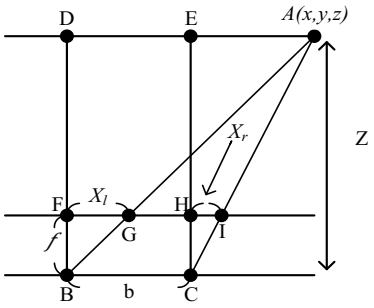

Fig. 3 Epipolar plane

$$\frac{x}{z} = \frac{x_l}{f} \quad (1)$$

$$\frac{x-b}{z} = \frac{x_r}{f} \quad (2)$$

$$z = \frac{bf}{x_l - x_r} \quad (3)$$

Here, f is the focal length, and the depth image was constructed by the set of z. In other word, each pixel value in the depth image corresponds to the depth of each point of the object in the real word.

C. Website

Users can monitor the tire tread depth through a website or Android phone. This system stores the measured tire tread depths in a MySQL database with the date and time of each measurement, which can be read in the form of a website programmed in PHP. Therefore, users can connect to this website using an APP on their phone or tablet to acquire a tire tread depth, and the date and time that it was recorded, as shown in Fig. 4.

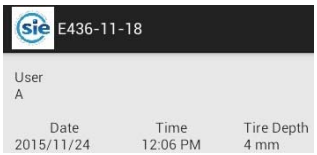

Fig. 4 The tread depth was shown in the smart phone

III. TIRE DEPTH ALGORITHM

Because a groove consists of two groove walls and a bottom, this study had to find the boundary between the surface of the main tread and the groove, and then to analyze the depth in the depth image along the normal direction of the boundary.

This study calibrated the parameters, including the stereoscopic image focal distance, with two cameras using image triangulation and Labview stereo vision. The distances between lens and the tire treads was calculated by Labview, and then the field of view of the cameras was transfer to a depth image, where the pixels value mean the distance between the corresponding points on the tire tread and the lens. The area inside the red rectangle in Fig. 5 is the ROI for analyzing the

tire tread depth, where $d1$ stands for the depth at the edge of the left tread surface, $d2$ stands for the depth at the bottom of the groove, and formula (4) can be obtained with tread depth dt.

Fig. 5 Region of interested in the tire image

$$dt = d2 - d1 \qquad (4)$$

The detailed calculation method is as follows. First, measure distance z between the camera and the tire treads using Labview's SGM algorithm [5]. Not all of the d1 pixel values of depth value Z calculated by the SGM function are the same in the images of the tread surface, and some will even be distinctly atypical. Therefore, the outlier pixels in the depth images were filtered using a median filter, and the depth images were enhanced using an image adjustment. To combine these pixels with similar value, using the traditional FCM method divided the depth image into many clusters. Then, the depth images were divided into clusters. Along the normal direction of the boundary of the groove, the tire tread depth was calculated according to the depth d1 and d2 using formula (4).

The detailed enhancement contrast and FCM methods are as follows.

A. Image Adjustment

An image adjustment was conducted using Matlab's image adjustment function [6], which could calculate the ratio of the difference between the pixel value and the smallest pixel value to the image range, and then redistributes the pixel values from zero to 255.

$$Ix(i,j) = \frac{x(i,j) - I\_min}{I\_max - I\_min} \times 255 \qquad (5)$$

Here, $x(i,j)$ stands for the pixel value; I_min stands for the smallest pixel value of the images; I_max stands for the largest pixel value of the images; and $Ix(i,j)$ stands for the pixel values redistributed.

B. FCM method

The FCM method can divide depth images into clusters. The basic FCM concept is to evaluate the membership ratio of the pixels in each cluster using a fuzzy membership function, as shown in formula (6), and then update the center of each cluster using the membership ratio, as shown in formula (7).

During actual operations, the original cluster centers of each cluster were assigned first, which were substituted into formula (6) to obtain the membership ratio. The cluster centers were then updated according to the membership ratio, and this iterative operation was repeated until the cluster center values converged.

$$\mu_{ij} = 1 / \sum_{k=1}^{c} \left(\frac{\|x_j - V_i\|}{\|x_j - V_k\|} \right)^2 \qquad (6)$$

$$V_i = \frac{\sum_{j=1}^{N} {\mu_{ij}}^2 x_j}{\sum_{j=1}^{N} {\mu_{ij}}^2} \qquad (7)$$

Here, $\{x_j\}$ stands for the j image pixel; N stands for the total number of image pixels; V_i stands for the i cluster center; images are divided into c clusters; and μ_{ij} stands for the membership ratio of the j pixel to the i cluster center.

IV. EXPERIMENTS

An experiment measured Bridgestone 185/65R14 B381 tires, including a new tire and two old worn ones. Each surface of the tires were divided into eight equal parts, and an image of the tire treads was captured at the center of each part.

Experiments were conducted with brightness levels of 4000 and 7500 lux. The Labview stereo vision SGM algorithm was used with various disparity wind sizes [7] (5, 7, 9, 11, 13, 15, 17, and 19) to determine the influence of the wind size on the measured tire tread depth. See Tables I–VI for results, where the value listed in these tables are in millimeters

TABLE I
LUX7500 NEW TIRE DEPTH

Wind Size	5	7	9	11	13	15	17	19
New Tread (a)	8	8	8	8	8	8	8	8
New Tread (b)	8	8	8	8	8	8	8	8
New Tread (c)	9	8	8	8	8	8	8	8
New Tread (d)	3	9	9	9	9	9	9	9
New Tread (e)	9	9	9	8	8	8	8	8
New Tread (f)	9	9	9	9	8	8	8	8
New Tread (g)	9	8	8	8	8	8	8	8
New Tread (h)	8	8	8	8	8	8	8	8

The actual tire tread depth was 8 mm.

TABLE II
LUX7500 OLD-1 TIRE DEPTH

Wind Size	5	7	9	11	13	15	17	19
Old-1 Tread (a)	4	4	4	4	4	4	4	4
Old-1 Tread (b)	4	4	4	4	4	4	4	4
Old-1 Tread (c)	4	4	4	4	4	4	4	4
Old-1 Tread (d)	4	4	4	4	4	4	4	4
Old-1 Tread (e)	4	4	4	4	4	4	4	4
Old-1 Tread (f)	4	4	4	4	4	4	4	4
Old-1 Tread (g)	4	4	4	4	4	4	4	4
Old-1 Tread (h)	4	4	4	4	4	4	4	4

The actual tire tread depth is 4 mm.

TABLE III
LUX7500 OLD-2 TIRE DEPTH

Wind Size	5	7	9	11	13	15	17	19
Old-2 Tread (a)	5	5	5	5	5	5	5	5
Old-2 Tread (b)	5	5	5	5	5	5	5	5
Old-2 Tread (c)	4	4	4	4	4	4	4	4
Old-2 Tread (d)	5	5	5	5	5	5	5	5
Old-2 Tread (e)	5	5	5	5	5	5	5	5
Old-2 Tread (f)	5	5	5	5	5	5	5	5
Old-2 Tread (g)	5	5	5	5	5	5	5	5
Old-2 Tread (h)	5	5	5	5	5	5	5	5

The actual tire tread depth is 5 mm.

TABLE IV
LUX4000 NEW TIRE DEPTH

Wind Size	5	7	9	11	13	15	17	19
New Tread (a)	8	8	8	8	8	8	8	8
New Tread (b)	8	8	8	8	8	8	8	8
New Tread (c)	9	9	9	9	9	9	8	8
New Tread (d)	9	8	8	9	9	9	9	8
New Tread (e)	9	9	9	9	9	9	9	9
New Tread (f)	9	8	8	8	8	8	8	8
New Tread (g)	9	9	8	8	8	8	9	9
New Tread (h)	8	8	8	8	8	8	8	8

The actual tire tread depth was 8 mm.

TABLE V
LUX4000 OLD-1 TIRE DEPTH

Wind Size	5	7	9	11	13	15	17	19
Old-1 Tread (a)	4	4	4	4	4	4	4	4
Old-1 Tread (b)	4	4	4	4	4	4	4	4
Old-1 Tread (c)	4	4	4	4	4	4	4	4
Old-1 Tread (d)	4	4	4	4	4	4	4	4
Old-1 Tread (e)	5	5	5	5	5	5	5	5
Old-1 Tread (f)	5	5	5	4	4	4	4	4
Old-1 Tread (g)	5	4	5	5	4	4	4	4
Old-1 Tread (h)	5	5	5	4	4	4	4	4

The actual tire tread depth is 4 mm.

TABLE VI
LUX4000 OLD-2 TIRE DEPTH

Wind Size	5	7	9	11	13	15	17	19
Old-2 Tread (a)	5	5	5	5	5	5	5	5
Old-2 Tread (b)	5	5	5	5	5	5	5	5
Old-2 Tread (c)	5	5	5	5	5	5	5	5
Old-2 Tread (d)	5	5	5	5	5	5	5	5
Old-2 Tread (e)	4	5	5	5	5	5	5	5
Old-2 Tread (f)	5	5	5	5	5	5	5	5
Old-2 Tread (g)	5	5	5	5	5	5	5	5
Old-2 Tread (h)	5	5	5	5	5	5	5	5

The actual tire tread depth is 5 mm.

When measured using the traditional contact tread depth meter, the actual depth of the tire treads of the new tire was 8 mm, and those of the first and second old tires were 4 mm and 5 mm, respectively.

Table I lists the depths of the tire treads of the new tire measured using the image triangulation of this system under 7500 lux. The correct tire tread depths could be acquired from seven of the eight tire tread images of the new tire within the range of wind size 13–19.

The correct depth value of 4 mm could be obtained from all the depth images of the tire treads of the first old tire listed in Table II after observing the influence of the wind size on the analysis of the tire tread images. A 1-mm error in the depth value of the tire treads of the second old tire occurred during the old-2 tread (c) image analysis listed in Table III, whereas the correct depth value could be obtained from the other seven images.

However, one mm error occurred in the analyses of the new tread (c, d, e, g) tire tread images of the new tire listed in Table IV when the wind size lay was 13–19 if the brightness was reduced to 4000 lux. In addition, false depths were found in the old-1 tread (e) image analyses of the first old tire. However, no false depths were found in the second old tires, as listed in Table V and Table VI, respectively.

In other words, the experiment results for the brightness and wind size indicated that multiple false depths were found when analyzing the tire tread images with a brightness level of 4000 lux. Therefore, better measurement results could be obtained when analyzing the tire tread images with a brightness of 7500 lux when the wind size was 13–19.

The results of the experiment also indicated that the correct tire tread depth could be obtained from seven of the eight images of the same tire.

V. CONCLUSIONS

The experiments in this study indicated that better measurement results could be obtained when analyzing tire tread images using a brightness level of 7500 lux and the Labview stereo vision SGM algorithm when the wind size was 13–19.

This study distinguished the boundary between the surface and groove of the main tire treads mainly using traditional image processing and FCM. The distance was obtained between the tire treads and camera lens, and the correct depth of the wall and groove of the main tire treads was found from the depth images using SGM with the majority decision strategy in the normal direction of this boundary, which was used to calculate the tire tread depth.

The experiments indicated that the correct tire tread depth could be obtained from seven of the eight images of the same tire. In other words, valid tire tread depth images could be acquired from the depth images. Furthermore, the correct tire tread depth could be analyzed from these images, which could then be uploaded to the phone or tablet of a user through the MySQL database.

REFERENCES

[1] H. Chen and Z. Xu. 3d map building based on stereo vision. In IEEE International Conference on Networking, Sensing and Control, ICNSC, 2006.

[2] The U.S.A department of transportation website.[Online].Available: https://www.fmcsa.dot.gov/regulations/title49/section/393.75/

[3] Ministry of transportation and communications R.O.C.website. [Online].Available: http://www.motc.gov.tw/ch/home.jsp?id=14&parentpath=0,2&mcustomize=news_view.jsp&dataserno=201309100006

[4] K.L.chung. Image Processing And Computer Vision, Tunghua, Inc., ISBN 978-957-483-697-0, 2014

[5] Birchfield, S. and Tomasi, C. Depth Discontinuities by Pixel-to-Pixel Stereo, IJCV, vol. 35(3), pp. 269-293, 1999.

[6] mathworks image processing toolbox website.[Online].Available: http://www.mathworks.com/help/images/ref/imadjust.html

[7] ni vision 2014 for labview help website.[Online].Available: http://zone.ni.com/reference/en-XX/help/370281W-01/imaqvision/imaq_stereo_correspondence__sg_block_matching/